Energy dependence of J/ψ production in pp collisions from the PACIAE model

Kai-Fan Ye,[1,2] Qiang Wang,[1] Jia-Hao Shi,[1] Zhi-Ying Qin,[1] Wen-Chao Zhang,[1,*] An-Ke Lei,[2] Zhi-Lei She,[3] Yu-Liang Yan,[4] and Ben-Hao Sa[4]

[1]*School of Physics and Information Technology, Shaanxi Normal University, Xi'an 710119, China*
[2]*Key Laboratory of Quark and Lepton Physics (MOE) and Institute of Particle Physics, Central China Normal University, Wuhan 430079, China*
[3]*School of Mathematical and Physical Sciences, Wuhan Textile University, Wuhan 430200, China*
[4]*China Institute of Atomic Energy, P. O. Box 275 (10), Beijing 102413, China*

(Received 19 October 2023; revised 24 January 2024; accepted 6 February 2024; published 12 March 2024)

In this work we investigate the J/ψ production in proton-proton collisions at the center-of-mass energy ($\sqrt{s}$) equal to 2.76, 5.02, 7, 8, and 13 TeV with the parton and hadron cascade model PACIAE 2.2a. It is based on PYTHIA but extended considering the partonic and hadronic rescatterings before and after hadronization, respectively. In the PYTHIA sector the J/ψ production quantum chromodynamics processes are selected specially and a bias factor is proposed correspondingly. The calculated total cross sections, the transverse momentum differential, and the rapidity differential cross sections of J/ψ in the forward rapidity region reproduce the corresponding experimental measurements reasonably well. In the mid-rapidity region, the double-differential cross sections at $\sqrt{s} = 5.02$, 7, and 13 TeV are also in a good agreement with the experimental data. Moreover, we interpolate the double-differential cross section as well as the total cross section of J/ψ in the mid-rapidity region at $\sqrt{s} = 8$ TeV, which could be validated if the experimental data are available.

DOI: 10.1103/PhysRevC.109.035201

I. INTRODUCTION

J/ψ is the lightest vector charmonium meson. The suppression of J/ψ production was proposed as a probe to investigate the hot and dense medium, named the quark-gluon plasma (QGP), created in ultrarelativistic nucleus-nucleus collisions [1]. The J/ψ production could also be suppressed due to the cold nuclear matter effects, such as modifications of nuclear parton distribution functions [2,3]. In order to disentangle the hot and cold medium effects, it is necessary to understand the J/ψ production in proton-proton (pp) collisions where the initial state effects are absent.

The hadronic J/ψ production mainly results from the gluon-gluon scattering into a $c\bar{c}$ pair in hard scattering and related initial- and final-state radiations, which is described with the perturbative quantum chromodynamics (pQCD). The hadronization of the c and $\bar{c}$ pair into J/ψ is a soft process, which cannot be dealt with by pQCD. The J/ψ production was extensively investigated at colliders such as the Tevatron [4–7], RHIC [8], and LHC [9–16]. Several theoretical approaches, such as the color singlet model [17], the nonrelativistic QCD model [18,19], and the color evaporation model [20,21], have been utilized to describe the experimental data. They differ mostly in the treatment of nonperturbative evolution of the $c\bar{c}$ pair into the bound state J/ψ. However, none of these models could simultaneously describe the polarization, the transverse momentum (p_{T}) spectrum, and the energy dependence of cross sections for J/ψ [13]. The J/ψ production was also investigated by Monte Carlo simulations. For example, in Refs. [22,23], the J/ψ production as a function of charged particle multiplicity in pp collisions at the center-of-mass energy ($\sqrt{s}$) equal to 7 and 13 TeV was investigated in the mid-rapidity region by PYTHIA 6.4 [24] and 8.2 [25], respectively. It was found that PYTHIA 8.2 could depict the correlation between the J/ψ yield and the charged-particle multiplicity ($dN_{\mathrm{ch}}/d\eta$) while PYTHIA 6.4 cannot do it well. This could be because the multiparton interaction is described differently between them. In Ref. [23], the correlation between the J/ψ yield and $dN_{\mathrm{ch}}/d\eta$ was also explored by the EPOS3 event generator [26,27]. In Ref. [28], the authors utilized a modified ultrarelativistic quantum molecular dynamics (UrQMD) transport model [29,30] to study the J/ψ suppression in high-multiplicity pp collisions at $\sqrt{s} = 7$ TeV.

Apart from the study in Refs. [22,23,28], we use a parton and hadron cascade model PACIAE 2.2a [31] without considering the polarization to investigate the J/ψ production in pp collisions at $\sqrt{s} = 2.76$, 5.02, 7, 8, and 13 TeV. In the PACIAE model, the J/ψ production QCD processes will be selected specially and a bias factor will be introduced for the simulated sample correspondingly. The calculated total cross sections, the differential cross sections as a function of the transverse

*wenchao.zhang@snnu.edu.cn

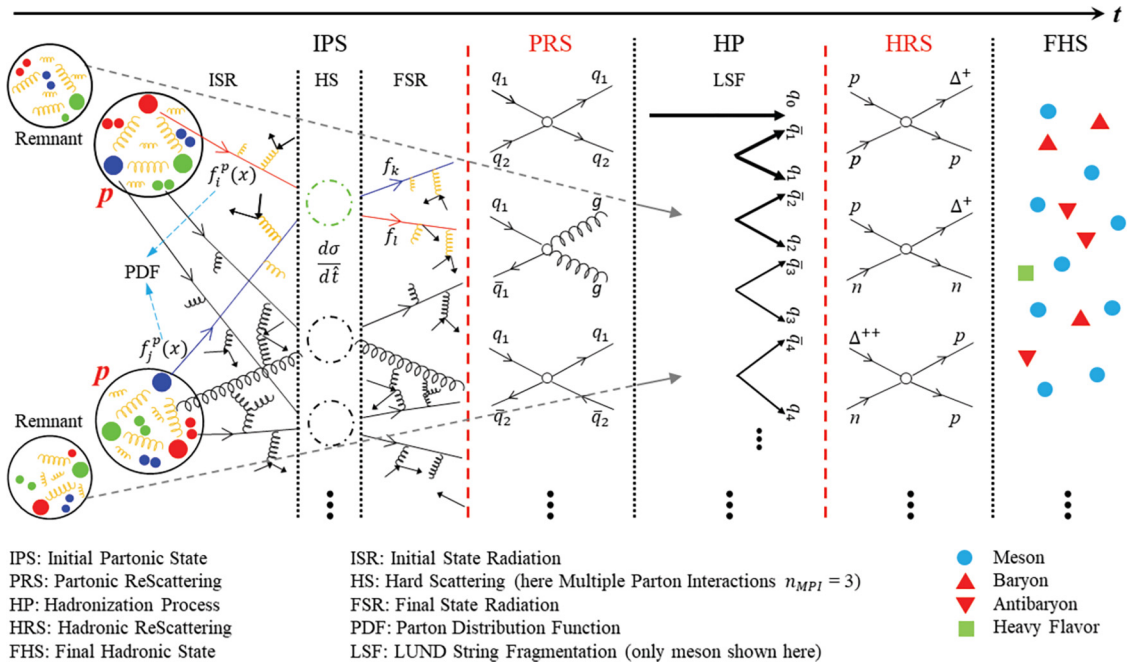

FIG. 1. A sketch of the physical routines in high-energy *pp* collisions [34].

momentum, and as a function of the rapidity of J/ψ in the forward rapidity region will be, respectively, compared to the corresponding experimental measurements. Meanwhile, at mid-rapidity the total and double-differential cross sections at $\sqrt{s} = 5.02$, 7, and 13 TeV will also be compared with the experimental data. Moreover, the total and double-differential cross sections of J/ψ at $\sqrt{s} = 8$ TeV will be interpolated in the mid-rapidity region.

This paper is organized as follows. In Sec. II, we briefly introduce the PACIAE model. In Sec. III, we describe the method to produce the simulated sample and to compare the sample with experimental data. In Sec. IV, results and discussions are presented. Finally, the conclusion is given in Sec. V.

II. THE PACIAE MODEL

The PACIAE 2.2a model is designed for elementary collisions. It is based on PYTHIA 6.4 but further considers the partonic rescattering before hadronization and the hadronic rescattering after hadronization. It divides the ultrarelativistic-energy *pp* collisions into four stages: parton initiation, parton rescattering, hadronization, and hadron rescattering. Figure 1 is a sketch of the physical routines in a high-energy *pp* collision.

In the first stage, the initial partonic states are created by the hard scatterings, the initial- and final-state radiations in PYTHIA with temporarily switching off the string fragmentation, breaking down the strings and splitting up the diquarks (anti-diquarks) randomly. This partonic matter then undergoes parton rescatterings, where the leading order (LO) pQCD parton-parton interaction cross sections [32,33] are employed. A K factor is introduced to consider higher-order effects and nonperturbative corrections for LO-pQCD parton-parton differential cross sections. After the parton rescattering, the partonic matter is converted into hadrons by the string fragmentation [24] or the coalescence model [34].

Then followed is the hadronic rescattering. Based on the hadron list after hadronization, two loops over i and j cycling through all hadrons are implemented. If the minimum approaching distance D between two straight-line trajectories of i and j particles satisfies $D \leqslant \sqrt{\sigma_{ij}^{\rm tot}/\pi}$, where $\sigma_{ij}^{\rm tot}$ is the total cross section of these two particles, the particles i and j may collide and the collision time t_{ij} is evaluated [35]. With the t_{ij} of all i-j pairs, the initial hadron-hadron collision time list is constructed. A collision with the least time is picked up from the list and implemented probably. The hadron list and collision time list are then updated [34]. With the repeat of these two steps until the collision time list is empty, the kinetic freeze-out happens. For the J/ψ hadronic rescattering, besides the elastic scattering, so far the following inelastic processes are considered [35,36]:

$$
\begin{aligned}
&J/\psi + n \to \Lambda_c^+ + D^-, \quad J/\psi + n \to \Sigma_c^+ + D^-,\\
&J/\psi + n \to \Sigma_c^0 + \bar{D}^0, \quad J/\psi + p \to \Lambda_c^+ + \bar{D}^0,\\
&J/\psi + p \to \Sigma_c^+ + \bar{D}^0, \quad J/\psi + p \to \Sigma_c^{++} + D^-,\\
&J/\psi + \pi^+ \to D^+ + \bar{D}^{*0}, \quad J/\psi + \pi^- \to D^0 + D^{*-},\\
&J/\psi + \pi^0 \to D^0 + \bar{D}^{*0}, \quad J/\psi + \pi^0 \to D^+ + D^{*-},\\
&J/\psi + \rho^+ \to D^+ + \bar{D}^0, \quad J/\psi + \rho^- \to D^0 + D^-,\\
&J/\psi + \rho^0 \to D^0 + \bar{D}^0, \quad J/\psi + \rho^0 \to D^+ + D^-.
\end{aligned}
$$

There are other models, e.g., the comover interaction model, etc., that also include hadronic rescatterings [37–47].

TABLE I. List of ALICE measurements for J/ψ productions.

	Forward rapidity		Mid-rapidity	
$\sqrt{s}$	Interval	Reference	Interval	Reference
2.76 TeV	$2.5 < y < 4$	[9]		
5.02 TeV	$2.5 < y < 4$	[16]	$-0.9 < y < 0.9$	[11]
7 TeV	$2.5 < y < 4$	[13]	$-0.9 < y < 0.9$	[12]
8 TeV	$2.5 < y < 4$	[14]		
13 TeV	$2.5 < y < 4$	[16]	$-0.9 < y < 0.9$	[15]

III. THE METHOD

The ALICE collaboration has published the inclusive J/ψ production in the forward rapidity region with $2.5 < y < 4$ in pp collisions at $\sqrt{s} = 2.76$, 5.02, 7, 8, and 13 TeV in Refs. [9,13,14,16]. The collaboration also presented the inclusive J/ψ productions in the mid-rapidity region with $-0.9 < y < 0.9$ in pp collisions at $\sqrt{s} = 5.02$, 7, and 13 TeV in Refs. [11,12,15]. They are listed in Table I. The inclusive J/ψ yield contains a prompt component, which includes the direct J/ψ production and the feed-down contribution from the decay of heavier charmonium states, as well as a non-prompt component from the weak decay of beauty hadrons.

In this paper, apart from the study performed by event generators such as PYTHIA 6.4, PYTHIA 8.2, EPOS3, and UrQMD [22,23,28], we investigate the J/ψ production in pp collisions at different energies with PACIAE 2.2a. In the model, a "menu" of subprocesses for the J/ψ production is composed with the sets of "MSEL=0" and "MSUB(i)=1, i=86, 87, 88, 89, 104, 105, 106". This especial setting is completely the same as that in PYTHIA 6.4. It corresponds to the following "color-singlet" processes, $gg \to J/\psi g$, $gg \to \chi_{0c} g$, $gg \to \chi_{1c} g$, $gg \to \chi_{2c} g$, $gg \to \chi_{1c}$, $gg \to \chi_{2c}$, $gg \to J/\psi\gamma$. The higher-mass excited states, like the χ_{0c}, χ_{1c}, and χ_{2c}, may subsequently decay to J/ψ. Since the $\psi(2S)$ production channel is not available in the PYTHIA 6.4 default processes, we did not consider the contribution of $\psi(2S)$ to J/ψ. As shown in Ref. [48], in the region with $p_T > 7$ GeV/c, the J/ψ production may be dominated by the "color-octet" processes. In this work, we only focus on the production of J/ψ in the low and intermediate p_T range below 7 GeV/c. Thus the "color-octet" processes are not considered. Relative to the default simulation without the above extra setting, the simulated results with the extra setting are bias samples. In order to remove this bias effect, for example, we rescale the cross sections in simulation with the first moment of the J/ψ p_T spectra and match it with the similarly rescaled cross section in experiment,

$$\frac{\frac{d\sigma_{J/\psi}}{dy}\Big|_{\rm sim}}{\int p_T \frac{d^2\sigma_{J/\psi}}{dp_T dy}\Big|_{\rm sim} dp_T} = \frac{\frac{d\sigma_{J/\psi}}{dy}\Big|_{\rm exp}}{\int p_T \frac{d^2\sigma_{J/\psi}}{dp_T dy}\Big|_{\rm exp} dp_T}. \quad (1)$$

Thus, in order to compare the simulated samples with the experimental data, we propose a bias factor,

$$B = \frac{\int p_T \frac{d^2\sigma_{J/\psi}}{dp_T dy}\Big|_{\rm exp} dp_T}{\int p_T \frac{d^2\sigma_{J/\psi}}{dp_T dy}\Big|_{\rm sim} dp_T} = \frac{\int p_T \frac{d^2\sigma_{J/\psi}}{dp_T dy}\Big|_{\rm exp} dp_T}{\int p_T \frac{d^2N_{J/\psi}}{dp_T dy} \cdot \frac{\sigma_{J/\psi}}{N_{J/\psi}}\Big|_{\rm sim} dp_T}, \quad (2)$$

which has to be multiplied to the simulated results. Here we have inserted the relation between the differential yield and differential cross section (see Appendix for details). In Eq. (2), $N_{J/\psi}$ is the total J/ψ yield in simulation; $\sigma_{J/\psi}$ is the total J/ψ cross section in one event returned by PACIAE 2.2a and is tabulated in Table II. Similar treatments are applied to the differential rapidity distribution of J/ψ.

In PACIAE, the model parameters are chosen as the default values in the PYTHIA 6.4 model, except for the K factor, which is determined by fitting the simulation to the experimental data in pp collisions at a given energy with a least-χ^2s method. For the J/ψ differential cross section as a function of p_T in the forward rapidity region, the χ^2 is defined as

$$\chi^2 = \sum_{i=1}^{N} \frac{\left[y^i - f(p_T^i; K)\right]^2}{(\Delta^i)^2}, \quad (3)$$

where N is the number of data points, y^i is the experimental value in the ith bin, $f(p_T^i; K)$ is the simulated value in the same bin, and Δ^i is the total error of the experimental data. Table III gives the χ^2 values divided by the number of degrees of freedom (χ^2/ndf) for different K factors at a given energy.

TABLE II. Summary of cross sections ($\sigma_{\rm sel}$) for specially selected J/ψ "color-singlet" process in pp collisions at various energies from PACIAE simulation. The last row lists the total J/ψ cross section in one event at a given energy. This cross section can be calculated by the weighted sum of the cross sections for the J/ψ selection process $\sigma_{\rm sel}$, with the weight taken as the product of the fraction of heavier charmonium state's radiatively decaying into J/ψ [i.e., branching ratio (BR)] and the sampling probability.

	$\sigma_{\rm sel}$ (μb)						
Processes	2.76 TeV	5.02 TeV	7 TeV	8 TeV	13 TeV	BR	Sampling probability
$gg \to J/\psi g$	32.871	62.654	64.798	83.623	132.548	100.0%	2.184%
$gg \to \chi_{0c} g$	241.830	499.519	533.856	700.603	1169.812	1.4%	21.054%
$gg \to \chi_{1c} g$	138.797	312.055	345.636	460.827	823.761	34.3%	5.000%
$gg \to \chi_{2c} g$	265.777	552.470	593.993	779.302	1302.222	19.0%	23.101%
$gg \to \chi_{0c}$	294.944	554.780	572.512	744.378	1202.169	1.4%	23.525%
$gg \to \chi_{2c}$	255.635	484.268	502.488	651.972	1060.098	19.0%	25.083%
$gg \to J/\psi\gamma$	0.929	1.872	1.856	2.588	4.232	100.0%	0.053%
$\sigma_{J/\psi}$ (μb)	28.631	57.349	60.822	79.524	132.111		

TABLE III. Summary of χ^2/ndf for different K factors at a given energy. The minimum χ^2/ndf is shown by boldface type.

	χ^2/ndf				
K	2.76 TeV	5.02 TeV	7 TeV	8 TeV	13 TeV
1.1	5.39/6	14.06/6	23.85/6	17.09/6	66.34/7
1.2	4.74/6	10.93/6	19.57/6	16.77/6	71.67/7
1.3	6.11/6	17.25/6	**16.62/6**	16.40/6	63.80/7
1.4	4.81/6	13.55/6	18.87/6	17.08/6	60.94/7
1.5	6.86/6	11.44/6	21.23/6	**13.40/6**	58.07/7
1.6	**3.46/6**	13.10/6	19.18/6	13.71/6	58.83/7
1.7	5.92/6	**10.92/6**	19.54/6	14.85/6	**54.86/7**
1.8	7.04/6	14.89/6	19.25/6	14.37/6	65.33/7
1.9	5.96/6	15.22/6	20.05/6	14.94/6	71.83/7

The best K factor at that energy is determined by minimizing the corresponding χ^2 values and is shown by boldface type. At a given collision energy, the K factor for the J/ψ production in the mid-rapidity region is assumed to be the same as that in the forward rapidity region.

IV. RESULTS AND DISCUSSION

Figure 2 shows the inclusive J/ψ cross sections from PACIAE (hollow symbols) at forward rapidity in pp collisions at $\sqrt{s} = 2.76$, 5.02, 7, 8, and 13 TeV, comparing with experimental data (solid symbols). The error bars attached to the data points represent the total uncertainties of the J/ψ cross sections. It is found that the simulations well describe the experimental data. Figure 3 presents the inclusive J/ψ cross sections as a function of rapidity in the forward region. In order to make the simulations comparable with experimental data, we employed the same p_T cut in the former as those applied in the latter at each energy. It is observed that the simulation (hollow symbols) well reproduces the corresponding experimental measurement (solid symbols).

As described in Sec. III, due to the especial selection of the J/ψ production processes in the simulation, the bias factor is introduced when comparing the simulation with experimental data. The energy dependencies of the bias factors introduced, respectively, for the J/ψ y and p_T distributions are presented in Fig. 4. It is shown that at a given energy the former is larger than the latter. In addition, for both cases the bias factor slightly decreases with energy. In order to guide the eye, we parametrize the dependence of B on energy with a fit function $B = a + b\ln(\sqrt{s}/\text{TeV})$, where a and b are free parameters. The fitted curves are also presented in the figure. The upper (lower) panel in Fig. 5 shows the J/ψ rapidity differential (total) inclusive cross sections as a function of $\sqrt{s}$ in the forward rapidity region. It is observed that the simulations

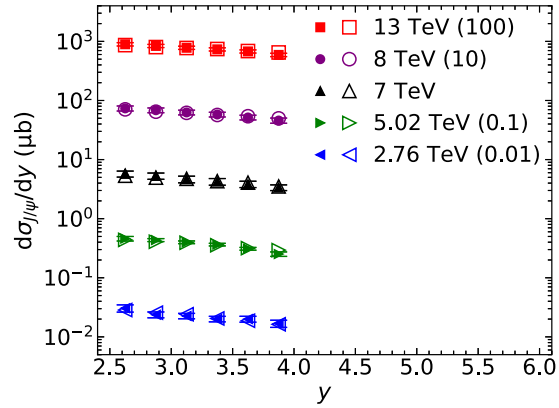

FIG. 3. Inclusive J/ψ single-differential cross sections as a function of y in pp collisions at $\sqrt{s} = 2.76$, 5.02, 7, 8, and 13 TeV. The solid symbols are experimental data taken from Refs. [9,13,14,16]. The hollow symbols are the results from the PACIAE model. The scaling factors in parentheses are used to improve visibility.

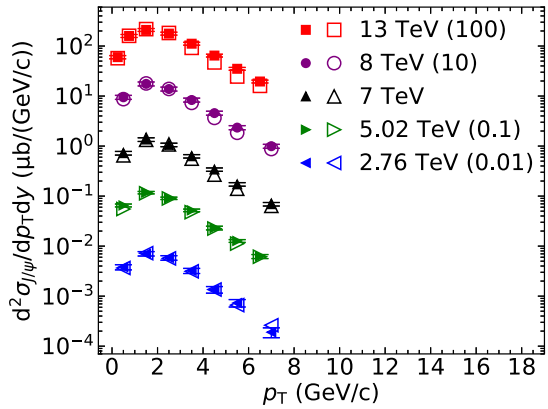

FIG. 2. Inclusive J/ψ double-differential cross sections as a function of p_T at forward rapidity in pp collisions with $\sqrt{s} = 2.76$, 5.02, 7, 8, and 13 TeV. The solid symbols are experimental data taken from Refs. [9,13,14,16]. The hollow symbols are the results from the PACIAE model. For better visibility, the p_T spectra are scaled by the numbers in parentheses.

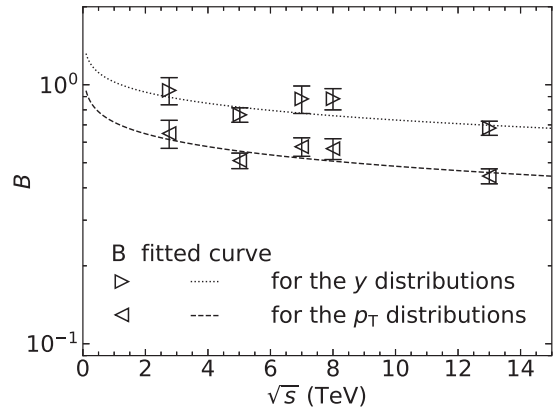

FIG. 4. The energy dependence of the bias factor in the forward rapidity region in pp collisions at $\sqrt{s} = 2.76$, 5.02, 7, 8, and 13 TeV. The left (right) triangles represent the bias factors calculated for the p_T (y) distributions. The dotted (dashed) curve represents the fitted function, $B = (1.025 \pm 0.057) + (-0.128 \pm 0.057)\ln(\sqrt{s}/\text{TeV})$ $[B = (0.717 \pm 0.084) + (-0.101 \pm 0.040)\ln(\sqrt{s}/\text{TeV})]$.

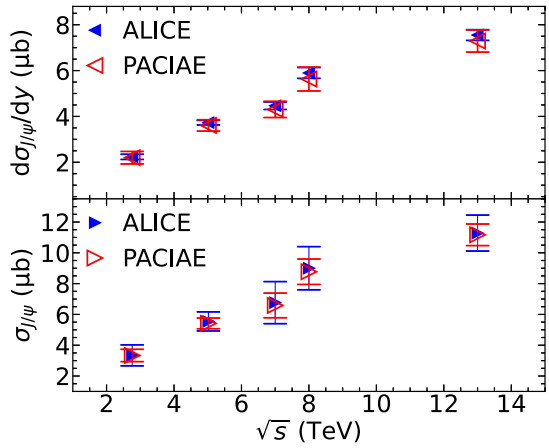

FIG. 5. Upper (lower) panel shows the J/ψ rapidity differential cross section (total cross section) as a function of $\sqrt{s}$ in the forward rapidity region in pp collisions. The solid (hollow) symbols represent the cross sections from the experimental data (the PACIAE model).

from the PACIAE model are in a good agreement with the experimental data. Moreover, there is a steady increase of the cross sections with the increasing collision energy. At a given energy, the total cross section is about a factor of 1.5 larger than the rapidity differential one. The bias factor for the J/ψ rapidity distribution is also 1.5 times larger than that for the p_T distribution. This factor is exactly the bin size in the forward rapidity region.

We use the same method as that in the forward rapidity region to determine the bias factor of the J/ψ double-differential cross sections in the mid-rapidity region. Figure 6 shows the energy dependence of the bias factor at mid-rapidity in pp collisions at $\sqrt{s} = 5.02$, 7, and 13 TeV. This energy dependence can be parametrized as $B = (0.764 \pm 0.159) + (-0.173 \pm 0.068)\ln(\sqrt{s}/\text{TeV})$. The bias factor at $\sqrt{s} = 8$ TeV is then interpolated with this parametrization formula. It is equal to 0.404 ± 0.032. Figure 7 presents the inclusive

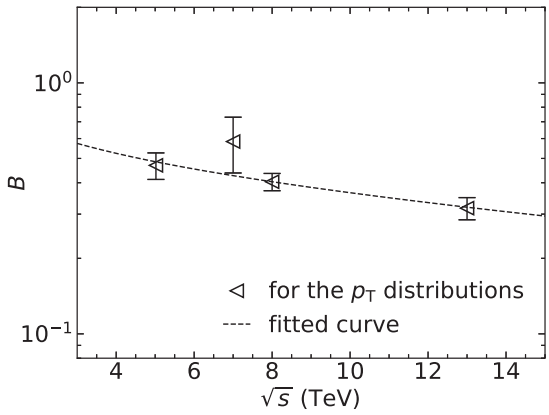

FIG. 6. The energy dependence of the bias factor in the mid-rapidity region in pp collisions at $\sqrt{s} = 5.02$, 7, and 13 TeV. The dashed curve represents the parametrization formula, $B = (0.764 \pm 0.159) + (-0.173 \pm 0.068)\ln(\sqrt{s}/\text{TeV})$. The bias factor at $\sqrt{s} = 8$ TeV is interpolated with this parametrization formula.

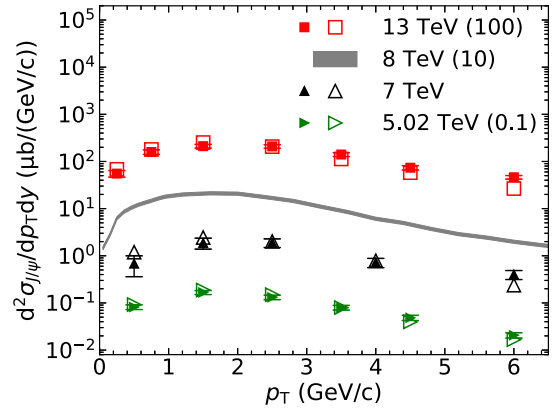

FIG. 7. Inclusive J/ψ double-differential cross sections as a function of p_T at mid-rapidity in pp collisions at $\sqrt{s} = 5.02$, 7, and 13 TeV. The solid symbols are experimental data taken from Refs. [11,12,15]. The hollow symbols are the results from the PACIAE model. The gray band represents the interpolated results from the PACIAE model in pp collisions at $\sqrt{s} = 8$ TeV. In order to improve the visibility, the rapidity distributions are scaled by the factors in parentheses.

J/ψ double-differential cross section as a function of p_T in the mid-rapidity region of $-0.9 < y < 0.9$ in pp collisions at $\sqrt{s} = 5.02$, 7, and 13 TeV. It is found that the simulations (hollow symbols) agree with experimental data (solid symbols) reasonably well.

In Sec. III, we determined the K factors by fitting the simulated J/ψ p_T differential cross sections to the experimental data in the forward rapidity region in pp collisions at $\sqrt{s} = 8$ TeV. Together with the assumption that the K factor at mid-rapidity is the same as that in the forward rapidity region (see Table III), we could generate the simulated sample for the J/ψ production in the mid-rapidity region in pp collisions at $\sqrt{s} = 8$ TeV. With the application of the bias factor interpolated at $\sqrt{s} = 8$ TeV (see Fig. 6) to the simulated sample, the double-differential J/ψ cross section at mid-rapidity in pp collisions at $\sqrt{s} = 8$ TeV is available. It is presented as the gray band in Fig. 7. Figure 8 shows the energy dependence of the simulated total inclusive J/ψ cross section at mid-rapidity in pp collisions at $\sqrt{s} = 5.02$, 7, and 13 TeV. At a given energy, the total cross section in simulation agrees with experimental data within uncertainties. The inclusive total J/ψ cross section at $\sqrt{s} = 8$ TeV is evaluated by integrating the double-differential cross section over p_T and y. The above interpolated J/ψ double-differential cross section and the total cross section in pp collisions at $\sqrt{s} = 8$ TeV could be validated if the experimental data are available.

V. CONCLUSIONS

In this paper, we have investigated the J/ψ production in pp collisions at $\sqrt{s} = 2.76$, 5.02, 7, 8, and 13 TeV with the parton and hadron cascade model PACIAE 2.2a. It is based on PYTHIA but differs from PYTHIA in the addition of the parton rescattering before hadronization and the hadron rescattering after hadronization. In the model the J/ψ pro-

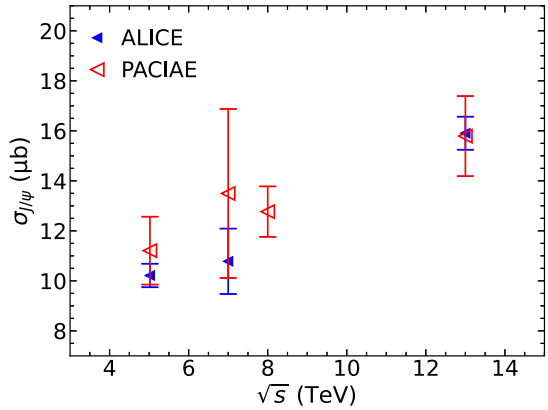

FIG. 8. Total inclusive J/ψ cross section at mid-rapidity in pp collisions with $\sqrt{s} = 5.02$, 7, and 13 TeV. The solid (hollow) symbols represent the cross sections from the experimental data (the PACIAE model). The total cross section at $\sqrt{s} = 8$ TeV is an interpolation based on the integration of the double-differential cross section over the mid-rapidity region.

duction QCD processes are selected specially and the bias factor is proposed and applied to the simulated sample correspondingly. The calculated J/ψ total cross section and the differential cross section as a function of $p_{\rm T}$ and y in the forward rapidity region agree with the corresponding experimental measurements reasonably well. In the mid-rapidity region, the double-differential cross sections of J/ψ at $\sqrt{s} =$ 5.02, 7, and 13 TeV also reproduce the experimental data. Moreover, the J/ψ double-differential cross section and the total cross section at $\sqrt{s} = 8$ TeV are interpolated. They could be validated if the experimental data are available.

We have noticed that the ALICE collaboration has published the results of J/ψ polarization in pp collisions at $\sqrt{s} = 7$ and 8 TeV [49,50]. We would like to see whether the PACIAE model could simultaneously describe the J/ψ polarization and $p_{\rm T}$ spectrum. Moreover, we realize the necessity of individually investigating the partonic and hadronic rescattering effects. These investigations will be presented in our next works.

ACKNOWLEDGMENTS

We would like to thank Prof. D.-M. Zhou, Prof. X.-M. Zhang, and Prof. G.-Y. Qin at Central China Normal University, and Prof. Y.-Q. Ma at Peking University for their valuable discussions. This work is supported by the research fund from the School of Physics and Information Technology at Shaanxi Normal University, by the Scientific Research Foundation for the Returned Overseas Chinese Scholars, State Education Ministry, by the Natural Science Basic Research Plan in Shaanxi Province of China (Program No. 2023-JC-YB-012), and by the National Natural Science Foundation of China under Grants No. 11447024, No. 11505108, and No. 12375135.

APPENDIX

In this Appendix, we present a detailed derivation of the relation between the J/ψ differential yield and differential cross section. The total J/ψ cross section in one event at a given energy in simulation, $\sigma_{J/\psi}$, can be expressed as

$$\sigma_{J/\psi} = \sigma^{ev}_{J/\psi} \frac{N_{J/\psi}}{N_{ev}} = \sigma^{ev}_{J/\psi} N^{\rm per}_{J/\psi}, \tag{A1}$$

where $N_{J/\psi}$ (N_{ev}) is the number of J/ψs (events) in the simulated sample, and $N^{\rm per}_{J/\psi} = N_{J/\psi}/N_{ev}$ is the number of J/ψs in one event. In this work, for each energy, N_{ev} is set to be 10^6. $\sigma^{ev}_{J/\psi} = \sigma_{J/\psi}/N^{\rm per}_{J/\psi}$ is the cross section of producing one J/ψ in one event. With Eq. (A1), the J/ψ differential cross section can be expressed as

$$\frac{{\rm d}^2\sigma_{J/\psi}}{dp_{\rm T}dy} = \frac{\sigma^{\rm ev}_{J/\psi}}{N_{\rm ev}} \frac{{\rm d}^2N_{J/\psi}}{dp_{\rm T}dy} = \frac{\sigma_{J/\psi}}{N_{J/\psi}} \frac{{\rm d}^2N_{J/\psi}}{dp_{T}dy}, \tag{A2}$$

i.e.,

$$\frac{1}{\sigma_{J/\psi}} \frac{{\rm d}^2\sigma_{J/\psi}}{dp_{\rm T}dy} = \frac{1}{N_{J/\psi}} \frac{{\rm d}^2N_{J/\psi}}{dp_{T}dy}. \tag{A3}$$

This is exactly the relation between the differential yield and differential cross section used in the simulation.

[1] T. Matsui and H. Satz, Phys. Lett. B **178**, 416 (1986).
[2] K. J. Eskola *et al.*, Eur. Phys. J. C **77**, 163 (2017).
[3] K. Kovařík *et al.*, Phys. Rev. D **93**, 085037 (2016).
[4] D. Acosta *et al.* (CDF Collaboration), Phys. Rev. D **71**, 032001 (2005).
[5] A. Abulencia *et al.* (CDF Collaboration), Phys. Rev. Lett. **99**, 132001 (2007).
[6] S. Abachi *et al.* (DØ Collaboration), Phys. Lett. B **370**, 239 (1996).
[7] B. Abbott *et al.* (DØ Collaboration), Phys. Rev. Lett. **82**, 35 (1999).
[8] A. Adare *et al.* (PHENIX Collaboration), Phys. Rev. Lett. **98**, 232002 (2007).
[9] B. Abelev *et al.* (ALICE Collaboration), Phys. Lett. B **718**, 295 (2012).
[10] B. Abelev *et al.* (ALICE Collaboration), Phys. Lett. B **748**, 472 (2015).
[11] S. Acharya *et al.* (ALICE Collaboration), J. High Energy Phys. 10 (2019) 084.
[12] K. Aamodt *et al.* (ALICE Collaboration), Phys. Lett. B **704**, 442 (2011).
[13] S. Acharya *et al.* (ALICE Collaboration), Eur. Phys. J. C **74**, 2974 (2014).
[14] J. Adam *et al.* (ALICE Collaboration), Eur. Phys. J. C **76**, 184 (2016).
[15] S. Acharya *et al.* (ALICE Collaboration), Eur. Phys. J. C **81**, 1121 (2021).
[16] S. Acharya *et al.* (ALICE Collaboration), Eur. Phys. J. C **77**, 392 (2017).
[17] R. Baier and R. Ruckl, Phys. Lett. B **102**, 364 (1981).

[18] G. T. Bodwin, E. Braaten, and G. P. Lepage, Phys. Rev. D **51**, 1125 (1995).
[19] G. T. Bodwin, E. Braaten, and G. P. Lepage, Phys. Rev. D **55**, 5853(E) (1997).
[20] H. Fritzsch, Phys. Lett. B **67**, 217 (1977).
[21] J. F. Amundson *et al.*, Phys. Lett. B **390**, 323 (1997).
[22] B. Abelev *et al.* (ALICE Collaboration), Phys. Lett. B **712**, 165 (2012).
[23] B. Abelev *et al.* (ALICE Collaboration), Phys. Lett. B **810**, 135758 (2020).
[24] T. Sjöstrand, S. Mrenna, and P. Z. Skands, J. High Energy Phys. 05 (2006) 026.
[25] T. Sjöstrand *et al.*, Comput. Phys. Commun. **191**, 159 (2015).
[26] K. Werner, Iu. Karpenko, T. Pierog, M. Bleicher, and K. Mikhailov, Phys. Rev. C **82**, 044904 (2010).
[27] K. Werner, B. Guiot, Iu. Karpenko, and T. Pierog, Phys. Rev. C **89**, 064903 (2014).
[28] T. Lang and M. Bleicher, Phys. Rev. C **87**, 024907 (2013).
[29] S. A. Bass *et al.*, Prog. Part. Nucl. Phys. **41**, 255 (1998).
[30] M. Bleicher *et al.*, J. Phys. G: Nucl. Part. Phys. **25**, 1859 (1999).
[31] D. M. Zhou *et al.*, Comput. Phys. Commun. **193**, 89 (2015).
[32] B. L. Combridge *et al.*, Phys. Lett. B **70**, 234 (1977).
[33] R. D. Field, *Applications of Perturbative QCD* (Addison-Wesley Publishing Company Inc., New York, 1989).
[34] A.-K. Lei *et al.*, Phys. Rev. C **108**, 064909 (2023).
[35] B. H. Sa *et al.*, Comput. Phys. Commun. **183**, 333 (2012).
[36] S. G. Matinyan and B. Muller, Phys. Rev. C **58**, 2994 (1998).
[37] S. Gavin, M. Gyulassy, and A. Jackson, Phys. Lett. B **207**, 257 (1988).
[38] R. Vogt, Phys. Lett. B **430**, 15 (1998).
[39] N. Armesto and A. Capella, Phys. Lett. B **430**, 23 (1998).
[40] C. Spieles, R. Vogt, L. Gerland, S. A. Bass, M. Bleicher, H. Stocker, and W. Greiner, Phys. Rev. C **60**, 054901 (1999).
[41] A. Capella, E. G. Ferreiro, and A. B. Kaidalov, Phys. Rev. Lett. **85**, 2080 (2000).
[42] Z. Lin and C. M. Ko, Phys. Rev. C **62**, 034903 (2000).
[43] A. Capella, L. Bravina, E. G. Ferreiro, A. Kaidalov, K. Tywoniuk, and E. Zabrodin, Eur. Phys. J. C **58**, 437 (2008).
[44] E. G. Ferreiro, Phys. Lett. B **749**, 98 (2015).
[45] N. Fischer and T. Sjöstrand, J. High Energy Phys. 01 (2017) 140.
[46] E. G. Ferreiro and J. P. Lansberg, J. High Energy Phys. 10 (2018) 094.
[47] E. G. Ferreiro and J. P. Lansberg, J. High Energy Phys. 03 (2019) 063.
[48] K.-T. Chao, Y.-Q. Ma, H.-S. Shao, K. Wang, and Y.-J. Zhang, Phys. Rev. Lett. **108**, 242004 (2012).
[49] B. Abelev *et al.* (ALICE Collaboration), Phys. Rev. Lett. **108**, 082001 (2012).
[50] S. Acharya *et al.* (ALICE Collaboration), Eur. Phys. J. C **78**, 562 (2018).